Published in "Journal of Neural Engineering 8(4): 046010, 2011"
which should be cited to refer to this work.

In vivo deployment of mechanically adaptive nanocomposites for intracortical microelectrodes

J P Harris[1,2,6], A E Hess[2,3,6], S J Rowan[1,2,4], C Weder[4,5], C A Zorman[2,3], D J Tyler[1,2] and J R Capadona[1,2,7]

[1] Department of Biomedical Engineering, CWRU, 2071 Martin Luther King Jr Drive, Wickenden Bldg, Cleveland, OH 44106, USA
[2] Rehabilitation Research and Development, L Stokes Cleveland VA Medical Center, 10701 East Blvd. Mail Stop 151 AW/APT, Cleveland, OH 44106-1702, USA
[3] Department of Electrical Engineering, CWRU 2123 Martin Luther King Jr Drive, Glennan Bldg, Cleveland, OH 44106, USA
[4] Department of Macromolecular Science and Engineering, 2100 Adelbert Road, Kent Hale Smith Bldg, CWRU, Cleveland, OH 44106, USA
[5] Adolphe Merkle Institute and Fribourg Center for Nanomaterials, University of Fribourg, Rte de l'Ancienne Papeterie, PO Box 209, CH-1723 Marly 1, Switzerland

E-mail: jeffrey.capadona@case.edu

Abstract

We recently introduced a series of stimuli-responsive, mechanically adaptive polymer nanocomposites. Here, we report the first application of these bio-inspired materials as substrates for intracortical microelectrodes. Our hypothesis is that the ideal electrode should be initially stiff to facilitate minimal trauma during insertion into the cortex, yet become mechanically compliant to match the stiffness of the brain tissue and minimize forces exerted on the tissue, attenuating inflammation. Microprobes created from mechanically reinforced nanocomposites demonstrated a significant advantage compared to model microprobes composed of neat polymer only. The nanocomposite microprobes exhibit a higher storage modulus ($E' = \sim 5$ GPa) than the neat polymer microprobes ($E' = \sim 2$ GPa) and can sustain higher loads ($\sim$12 mN), facilitating penetration through the pia mater and insertion into the cerebral cortex of a rat. In contrast, the neat polymer microprobes mechanically failed under lower loads ($\sim$7 mN) before they were capable of insertion into cortical tissue. Further, we demonstrated the material's ability to morph while in the rat cortex to more closely match the mechanical properties of the cortical tissue. Nanocomposite microprobes that were implanted into the rat cortex for up to eight weeks demonstrated increased cell density at the microelectrode–tissue interface and a lack of tissue necrosis or excessive gliosis. This body of work introduces our nanocomposite-based microprobes as adaptive substrates for intracortical microelectrodes and potentially for other biomedical applications.

S Online supplementary data available from stacks.iop.org/JNE/8/046010/mmedia

[6] These authors contributed equally to this work.
[7] Author to whom any correspondence should be addressed.

1. Introduction

Intracortical microelectrodes for neural unit recording have led to many significant insights into the behaviour of the brain in animal models (Nicolelis 2003, Schwartz 2004). There have been several notable efforts to develop probes that can be implanted chronically in humans to directly interface with the brain to achieve command, control and feedback in many clinical applications (Kennedy *et al* 2004, Hochberg *et al* 2006). Intracortical interfaces that can be implanted and remain stable for many years offer many significant opportunities to improve human health, as well as our understanding of the brain. Unfortunately, at this time, this technology is not feasible for wide-scale clinical applications due to the variability in the reliability of the recordings over both short and long time periods, regardless of the type of electrode used (Ward *et al* 2009).

While it has been shown that intracortical microelectrodes can record the activity of individual or small populations of neurons early after implantation (Buzsáki 2004, Schwartz 2004), challenges still remain in maintaining the ability to record neural signals from individual or small groups of neurons for extended periods (McConnell *et al* 2009, Ward *et al* 2009, Williams *et al* 1999). This is largely attributed to the inflammatory response initiated by the trauma of implantation, and the foreign body reaction spanning the life of the chronically implanted microelectrode (Polikov *et al* 2005, He and Bellamkonda 2007, Leach *et al* 2010). Support for the importance of reducing the chronic inflammatory response to penetrating neural microelectrodes has been reported previously in both *in vitro* and *in vivo* models (Polikov *et al* 2005, 2006). Both of these systems demonstrate electrode encapsulation by neural inflammatory cells, and significant reduction in the number of neurons at the electrode tissue interface ('neuronal dieback'). Although the dominant mechanism is still being debated, it is important to point out that the ability of cortical microelectrodes to record from individual neurons is directly related to the proximity of viable neurons and the characteristics of non-neural, encapsulation tissue between the electrode and neuron (Biran *et al* 2005).

Traditionally, microelectrodes have been composed of metals, silicon and/or ceramics. These materials have a high mechanical stiffness (high modulus) relative to brain tissue. While the high modulus has enabled facile electrode implantations (Szarowski *et al* 2003), the stiffness difference between brain tissue (∼6 kPa) and typical electrode material (∼200 GPa) results in chronic shear and differential motion between the microelectrode and the neurons (Subbaroyan *et al* 2005). Previous research with *in silico* modelling and *in vivo* studies has indicated that indwelling microelectrodes become mechanically coupled to the brain tissue and exert forces on local populations of cells (Lee *et al* 2005, Subbaroyan *et al* 2005, McConnell *et al* 2007). The effects of the mechanical mismatch are thought to play a significant role in the cell-mediated inflammatory response impacting the glial scar, neuronal health and the microelectrode–cortical tissue interface (Williams *et al* 2007, Polikov *et al* 2005, He and Bellamkonda 2007, Leach *et al* 2010).

Several research groups have attempted to investigate the effects of mechanical mismatch between the microelectrodes and the cortical tissue, and many have developed microelectrode substrates and substrate coatings from materials such as polyimide, SU-8, polydimethylsiloxane (PDMS) and parylene that are more compliant than materials traditionally used to create electrodes (Rousche *et al* 2001, Subbaroyan and Kipke 2006, Takeuchi *et al* 2005, Wester *et al* 2009, Fernandez *et al* 2009, Mercanzini *et al* 2009, Lu *et al* 2009). However, in general, these materials have had limited success in attenuating glial scar formation or improving neural recordings. A drawback to most of these studies is that such materials still have Young's moduli six orders of magnitude larger than that of the brain (Takeuchi *et al* 2005, Lee *et al* 2004, Nikles *et al* 2003, Takeuchi *et al* 2004, Wester *et al* 2009). Additionally, the slight decrease in the stiffness of these polymeric-based microelectrodes results in difficulties in implanting the microelectrodes (Takeuchi *et al* 2005, Kozai and Kipke 2009, Lee *et al* 2003, Kee-Keun *et al* 2004), requiring insertion shuttles that can cause increased volumes of tissue damage during insertion and retraction (Kozai and Kipke 2009).

Therefore, we hypothesize that the ideal microelectrode should be composed of a material that is initially stiff to facilitate insertion into the cortex, yet becomes mechanically compliant to match the stiffness of the brain tissue, to minimize forces exerted on the tissue and to attenuate inflammation around the implant. To this end, we have recently developed a new class of bio-inspired, chemo-responsive, mechanically-adaptive polymer nanocomposite (NC) that can controllably and selectively be switched between stiff and compliant states (Capadona *et al* 2007, 2008, 2009, Shanmuganathan *et al* 2009, 2010a, 2010b, van den Berg *et al* 2007). The bio-inspired adaptive NC material design was based on the dermis of the echinoderm *holothuroidea* (sea cucumber). These invertebrates feature soft connective tissues with mutable mechanical properties; the animal can switch between low- and high-stiffness states on a sub-second time scale. Our materials exhibit this behaviour by mimicking the architecture and proposed switching mechanism at play in the sea cucumber dermis by utilizing a polymer NC consisting of a controllable structural scaffold of rigid cellulose nanofibres embedded within a soft polymeric matrix. When the nanofibres percolate, they interact with each other through hydrogen bonding and form a nanofibre network that becomes the load-bearing element, leading to a high overall stiffness of the NC. When combined with a polymer system which additionally undergoes a phase transition at physiologically relevant temperatures, a contrast of over two orders of magnitude for the tensile elastic modulus is exhibited. Initial material characterization has demonstrated that the polymer NC reduces its tensile storage modulus from ∼5 GPa to 12 MPa within 15 min upon exposure to simulated physiological conditions in artificial cerebral spinal fluid (ACSF) at 37 °C (Shanmuganathan 2010, Capadona *et al* 2008, 2009). Additionally, advanced bioMEMS fabrication processes have been developed to create cortical microprobes from this novel material (Hess *et al* 2009, 2011).

Here, we report on the first demonstration of the application of our mechanically dynamic material towards intracortical microelectrodes. This study shows that the stiffness of the NC facilitates insertion into the cortex of a living rodent, the NC mechanically morphs within the animal to achieve a compliant state more similar to the mechanical properties of the brain, and the NC can integrate within the cortical tissue over many weeks.

2. Materials and methods

2.1. Device fabrication

NC implants consisted of poly(vinyl acetate) and cellulose nanocrystals derived from tunicates (tunicate whiskers or whiskers) that were created by casting films from a dimethylformamide (DMF) solution of the polymer and whiskers (Capadona *et al* 2008). Poly(vinyl acetate) (PVAc, weight-average molecular weight, MW = 113 000 g mol^{-1}; density, d = 1.19 g cm^{-3}) was purchased from Sigma-Aldrich. The isolation of cellulose whiskers largely followed our published protocols with minor modifications (van den Berg *et al* 2007). NC films consisted of 15% w/w tunicate whiskers, and the films were used to create sheets via compression-molding in a hot press (Carver, Wabash, IN) to yield 53–110 μm thin films, depending on the experiment. Subsequently, two types of device were created: one for mechanical testing and buckling tests and another for insertion force measurements and histology.

Starting with compression-molded sheets, for both types of device, the NC sheets were cut into the appropriate shapes. For insertion force and histology, 100 μm thick sheets were cut into 3 mm long probes that were 200 μm wide with an approximately 45° angle tip. Probes for mechanical testing and buckling tests were created from a solution-cast poly(vinyl acetate)-tunicate whisker film compressed to a specified thickness (53 μm for buckling tests, 110 μm for mechanical measurements) and weakly adhered to a bare Si wafer by applying gentle pressure and heating on a hotplate set to 70 °C for 3 min. Using a direct-write CO_2 laser at a laser power of 0.5 W, speed of 56 mm s^{-1} and resolution of 1000 pulses per inch (Hess *et al* 2009, 2011), microprobes for mechanical testing were fabricated as beams 6 mm in length and 180–210 μm in width. For buckling testing, beams with a tip opening of 30° were cut using the same settings for the laser (3 mm in shank length, 125 μm in width, 53 μm thick). Neat polymer probes for buckle testing were fabricated to a similar size (3 mm in shank length, 125 μm wide and 55 μm thick) from spin-cast films. Neat PVAc films were fabricated by first dissolving 30 g PVAc in 50 mL DMF. Approximately 5 mL solution was statically dispensed onto a bare Si wafer, and then spin-cast onto the wafer at a spin speed of 2000 rpm for 30 s. The film was then dried in a vacuum oven for 4 h at 65 °C. Films were then immersed in DI water to aid in peeling them from the wafer. After drying overnight under ambient conditions, neat PVAc microprobes were laser-patterned using the same parameters as were developed for patterning the NC microprobes.

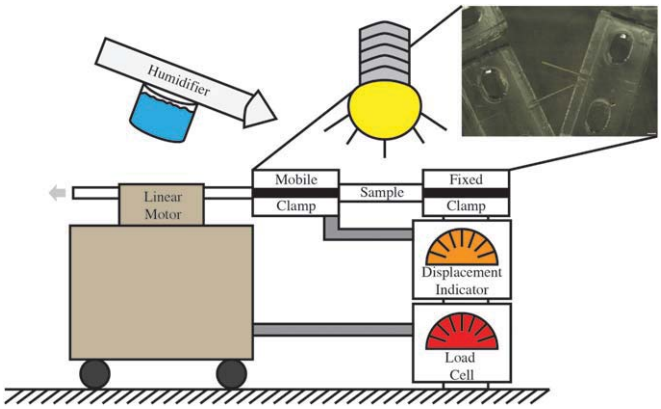

Figure 1. Diagram of MT instrumentation. Sample is held between two clamps where a load is applied to the sample, and both force and displacement are measured. The light and humidifier maintain the conditions similar to that within the rodent. The digital image depicts the model microprobes attached to the clamp (scale = 1 mm).

Separately, acrylic mounts designed to serve as the sample clamp during tensile testing were also fabricated and marked with an identification number and two lines indicating where the sample would be attached to the mount. A 1.5 mm long portion at one end of the NC samples was adhered to the acrylic mount using a cyanoacrylate-based adhesive, leaving a 4.5 mm long cantilever structure hanging from the mount (figure 1, digital image). After curing the adhesive overnight, the width and thickness of each sample were measured under a microscope and recorded along with the identifying number.

2.2. Surgical procedures

The same surgeon performed all procedures to minimize variability. The Case Western Reserve University Institutional Animal Care and Use Committee (CWRU IACUC) approved all procedures and all efforts to minimize the pain and discomfort of the animals were employed.

Sprague-Dawley rats weighing between 200 and 340 g were used for all experiments. Ketamine (80 mg kg^{-1}) and xylazine (10 mg kg^{-1}) provided anaesthesia induction via intraperitoneal injection (IP). When the animal was unresponsive to a toe pinch, the animal was prepared for surgery via head shaving and eye protection with ocular lubricant. Upon transfer of the animal to the stereotaxic frame fitted with a gas mask, the animal was ventilated with oxygen. Vitals were measured by a pulse oximeter attached to the hind limb paw. The animal was kept warm via a circulating water mat. When the animal began to whisk, reacted to toe pinch, or exhibited a raised heartbeat, the introduction of isoflurane (1–3%) into the oxygen flow maintained a surgical level of anaesthesia.

Access to the brain was gained by first creating a midline incision via a scalpel. Cotton swabs were used to move periosteum from the skull, and either a 3 mm biopsy punch or dental drill with stainless steel burr bit was used to remove the bone of the skull. Both types of openings were approximately

centred at 3 mm lateral from the midline and 4.5 mm caudal to the bregma. After opening the skull, the dura was removed using a fine 45° angle microprobe and fine forceps using a surgical microscope. Implants were attached to ceramic forceps tips, and implants were manually lowered to near the surface of the brain. A computer-controlled mechanical inserter controlled by a custom LabView 7.1 program inserted implants 2–3 mm into the brain at 2 mm s^{-1}. For microtensile testing (MT), implants were inserted into the brain with a micromanipulator instead of the computer.

In the case of animals used for histology (chronic survival animals), probes were left implanted in the animal. The skull was sealed with Kwik-Sil (WPI, Inc. Sarasota, FL) followed by dental cement adhered to three stainless steel screws implanted into the brain. The skin of the scalp was sutured closed over the dental cement and closely monitored for recovery.

2.3. Mechanical test procedures

2.3.1. Microtensile testing setup. Samples were implanted in the rat cortex for 1–30 min, then removed and immediately inserted into the microtensile tester (MT) that had previously been validated (Hess *et al* 2009, 2011). A computer-controlled, custom-built MT (figure 1) was utilized to measure the stress–strain relationship of NC samples that were used for *in vivo* experiments. The samples were gripped over a length of 1.5 mm on each end between acrylic blocks clamped by metal bolts, leaving a gauge length of 3 mm. One grip was anchored to an immobile structural component of the MT, and the other grip was attached to the drive rod of a linear piezomotor that applied a strain to the sample. The displacement distance was measured with an indicator with a resolution of 0.5 mm, and the force required to pull the sample was measured with a load cell with a resolution of 49 mN. The setup was computer-controlled via data acquisition software.

Each sample was tensile tested by straining at a rate of 8.9 mm s^{-1} until failure. The time from sample removal from the brain until completion of tensile test was recorded, typically between 3 and 4.5 min. After testing was completed, the stress and strain were calculated and the Young modulus was determined from the slope of the curve in the initial linear portion of the stress–strain curve.

2.3.2. Moisture and temperature maintenance. In order to keep the environmental conditions of the test setup similar to those of the biological environment of the implant, considerations were made for temperature and humidity. Temperature was controlled with the radiant heat from a focused light source using a thermocouple placed near the sample to set the local temperature to 37 °C. A fluid mist, via a commercial airbrush, maintained the humidity of the environment to prevent sample drying (Humidifier, figure 1). This is important as moisture is the primary stimulus of changing the mechanical properties of the NC. The effects of using or not using the humidifier were examined using dry and wet samples to examine the effect of the humidifier on mechanical testing results.

2.3.3. Dimensional changes due to swelling. To determine the cross-sectional dimensions of implanted samples for stress calculations, sample thickness and width were measured before and after soaking samples similar to the implanted samples in artificial cerebrospinal fluid (ACSF) for 30 min at 37 °C. The width or thickness of dehydrated samples was measured under a light microscope before the samples were immersed in ACSF at a temperature of 37 °C. After 30 min, the width and thickness of the samples were measured again. The percentage change for each dimension was calculated and used to calculate the cross-sectional dimensions of implanted samples.

2.4. Insertion force measurements

A computer-controlled mechanical inserter was used to insert implants 2–3 mm into the brain at 2 mm s^{-1} (as described above). The load cell was calibrated before each use via loading the load cell with determined weights, creating a voltage-force calibration curve. The computerized setup controlled a stepper motor outfitted with an optical encoder to track the position of the stepper motor while a load cell was mounted on the front of the stepper motor to record the forces during the insertion. The data acquisition board, synchronized to a motion control board, allowed for synchronous recording of position and load cell voltage. Data from a single insertion were post-processed to use the calibration curve to convert recorded voltage into force. Graphs and measurements of force versus position were used to determine the needed force for insertion as determined by the first peak in the insertion graph after the artefact from the initiation of movement (Jensen *et al* 2006, Paralikar *et al* 2006, Najafi and Hetke 1990).

2.5. Buckling load calculations

Following the analysis of insertion force data, statistical analysis was completed in the statistical package R (R Foundation for Statistical Computing, Vienna, Austria) (R Development Core Team 2009). An analysis was performed to analyse the distribution of forces and the force needed to insert into the brain. The 95% confidence level and required insertion force were computed using a *t*-distribution and analysis of the mean and standard deviation of observed data.

From the computed force to implant, the microprobe modulus was predicted by Euler's buckling formula (see below and Najafi *et al* (Najafi and Hetke 1990)). The parameter space was graphically investigated using Matlab R2009b (MathWorks, Natick, MA) by varying device length, width and thickness and insertion force predicted.

2.6. Buckle testing

During buckle testing, a video camera connected to a surgical scope recorded the insertion and retraction movements. The implants used had a 3 mm long shaft and were 125 μm wide with a thickness of 53 μm (NC) or 55 μm (neat polymer), both with a 30° opening angle. After 3 min, the implanted NC microprobes were removed from the brain tissue via the computer-controlled motor and manually moved to a new

insertion site. Immediately, the computer-controlled inserter was initiated to lower the probe into the brain at 2 mm s^{-1}. Between repeated insertions, the brain was not continually hydrated in order to minimize sample wetting by exogenous applied saline.

2.7. Histology

As a preliminary examination into the chronic response to the NC, a pair of animals was implanted with the NC microprobe and was euthanized after four or eight weeks to examine histology of the brain–implant interface. Following anaesthesia induction, transcardial perfusion was performed via a mechanical pump with approximately 500 mL of Dulbecco's phosphate-buffered saline followed by 250 mL of 10% buffered formalin fixing the tissue. The extracted brain was placed in formalin for 24 h, after which the brain was then transferred to fresh formalin where it remained for up to one week, until it was cryoprotected in 30% sucrose solution. To perform slicing of the brains, they were frozen in embedding molds (Electron Microscopy Products, Hatfield, PA) containing an optimal cutting temperature (OCT) compound (Sakura, Tokyo, Japan) that were then mounted and sectioned horizontally using a cryostat to create 30 μm thick slices. Following a standard haematoxylin and eosin (H+E) protocol, slices were stained, mounted and cover-slipped. Briefly, sections were rinsed in distilled water, and nuclei were stained with the haematoxylin. Following a rinse in tap water, tissue was differentiated with acid alcohol and rinsed in tap water. Finally, samples were stained with eosin for 2 min, then dehydrated and mounted (Lillie 1965). Separate slices were counterstained with 4′,6-diamidino-2-phenylindole (DAPI) dilactate (Invitrogen, Carlsbad, CA) at room temperature. All slices were imaged via a microscope outfitted with a greyscale CCD camera.

3. Results

3.1. Microprobe insertion into rat cortex

Implants fabricated from the PVAc/cellulose nanowhisker NC or, for the purpose of comparison, the neat PVAc polymer, were attached to ceramic forceps tips and manually lowered to near the surface of the brain. They were then advanced by computer control 3 mm towards the exposed brain at 2 mm s^{-1}. The implantation path typically exhibited a slight motion start artefact; an example can be seen in the first peak of figures 2(a) and (b). Generally, there was no increase in force before the microprobe came into contact with the surface of the brain. As the pia mater was indented, the force exerted on the tissue grew prior to the puncture of either the pia mater tissue (microprobe insertion through the tissue, figure 2(a)), or microprobe failure (material buckling, figure 2(b)). Video examples of an insertion and a buckle can be seen in the supplemental material available at stacks.iop.org/JNE/8/046010/mmedia (see below for a full explanation of the videos and still frames).

In the case of the NC microprobe, the pia was punctured, allowing the microprobe to penetrate into the brain, facilitating implantation when the force exerted was lower than 14 mN

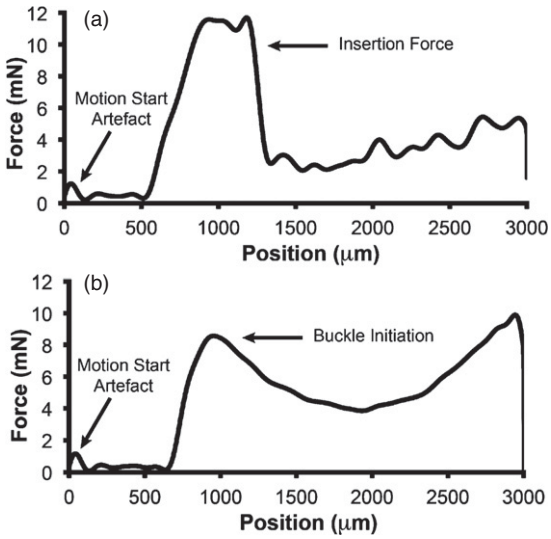

Figure 2. The insertion force was recorded as a function of microprobe position during all microprobe insertion trials. Representative trials of both the insertion of (a) a 3 mm long NC microprobe into the dura-removed cortex at a rate of 2 mm s^{-1}, and (b) the buckling of a 3 mm long neat PVAc microprobe upon failed insertion into the dura-removed cortex at a rate of 2 mm s^{-1}.

(figure 2(a)). After microprobe implantation was achieved, the force was quickly relaxed. After insertion, the microprobe continued to advance through the cortex, generating increased resistance against the microprobe, as depicted graphically by the second gradual rise (∼1500–3000 μm) in force after the initial insertion.

Under identical conditions, the neat PVAc polymer microprobes created for the purpose of comparison failed to penetrate the pia mater, but first bent and eventually buckled when the force exceeded 5.6 mN (figure 2(b)). The bowing out and eventual buckling of the microprobe resulted in a reduction in measured force where the buckling force was less than the required penetration force. In this case, the pia continued to indent as the microprobe was unable to penetrate the tissue, causing a second rise in force after the initial insertion or buckling event. We defined the maximum force as the force before the microprobe starts bowing out.

3.2. Dry NC modulus measurements

Displacement and force data were converted to strain and stress, respectively, by dividing displacement by the initial length, and dividing force by the initial cross-sectional area of the sample, respectively:

$$\varepsilon = \frac{d}{l_0} \tag{1a}$$

and:

$$\sigma = \frac{F}{w \cdot t}, \tag{1b}$$

where ε is the strain, d is the displacement measured by the indicator, l_0 is the initial gauge length (3 mm), σ is the sample stress, F is the force measured by the load cell, w is the sample width and t is the sample thickness.

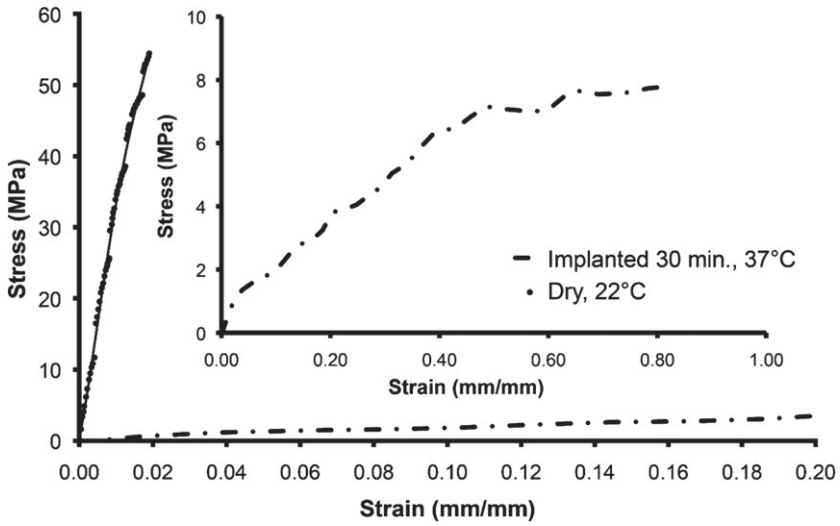

Figure 3. Stress–strain plots for both pre-inserted dynamic microprobes (dry, room temperature; $E = 3411$ MPa) and the identical composition of microprobe that had been implanted in living rat cortex (30 min implantation, explanted and tested at 37 °C; $E = 33$ MPa). The inset shows the stress–strain plot of the explanted sample on a different scale.

First, a dry NC microprobe sample was tested at room temperature to confirm the as-fabricated sample properties with our previous studies (Hess *et al* 2009, Capadona *et al* 2008, Shanmuganathan *et al* 2009, 2010a, 2010b). The Young modulus (E) of the sample is defined as the slope of the linear portion of the stress–strain curve. Using our test setup, the Young modulus was measured to be 3411 ± 98 MPa (number of samples $n = 5$ for this composition, figure 3), consistent with that previously reported (Hess *et al* 2011).

3.3. In vivo mechanical switching

To confirm that the NC microprobes remained mechanically dynamic upon implantation into the rat cortex, as previously shown *in vitro* for this bio-mimetic design (Capadona *et al* 2008), we explanted microprobes and re-examined their Young's modulus using our microtensile device (figure 3). Implantation into the rat cortex reduced the Young modulus of the NC by several orders of magnitude.

The *ex vivo* Young's modulus of the mechanically dynamic microelectrodes was plotted as a function of the implantation time (figure 4). There was no significant difference between samples that had been implanted for 5, 15 or 30 min, which collectively had a Young's modulus of 32 ± 13 MPa (figure 4). There was no statistical difference between data collected from MT and dynamic mechanic analysis (DMA) after 15 min of immersion (Shanmuganathan 2010). The time required for the setup of the tensile test plus the time required to strain the sample to break generally required 3–4.5 min after removal from the brain.

3.4. Examination of ex vivo modulus testing moisture

If allowed to dry upon explanting from physiological conditions, the reinforcing network within the mechanically dynamic NCs will return to their original stiff state (Capadona *et al* 2008). Therefore, to ensure an accurate measurement

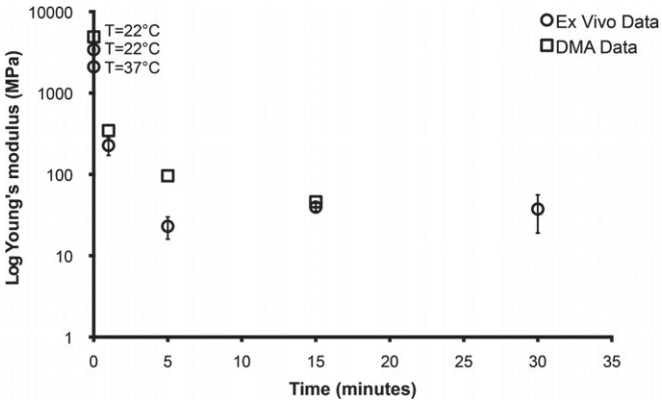

Figure 4. The Young modulus of the mechanically dynamic materials was measured with a DMA (open squares; bulk materials(Shanmuganathan 2010)) and with MT (open circles; explanted microprobes) to confirm mechanical switching from stiff to compliant. DMA samples were placed into a submersion clamp with ACSF preheated to 37 °C (Shanmuganathan 2010) while microprobes were implanted into the rat cortex and explanted for MT testing. The x-axis indicates the time of exposure to either ACSF or implanted in the rat cortex, respectively.

of the explanted modulus, materials were humidified via a fluid mister using water to prevent drying. To examine the effect of the fluid misting on measured samples, a sample was repeatedly tested before, during and after the application of a misting spray. In the case of a dry NC sample, the modulus was not statistically different between before and during humidifier application over 6 min (data not shown). After the 6 min of continued misting, the modulus did become significantly different from the modulus before or during humidifier application ($p = 0.03$, two-sample t-test), though the modulus only decreased by at most 10% after exposure to the humidifier moisture. This modulus decrease could be from the applied moisture, or the decrease could also be due to the sample being taken very slightly out of the

elastic region causing a reduction in the measured modulus. Alternatively, the difference could be from an increase in temperature after the humidifier was turned off, as temperature was not controlled in these tests. Further tests were performed to examine the effects of the humidifier (data not shown). After determining a setting at which the humidifier would contribute a minimal reduction in the Young modulus of the NC, the effect of the mister on wet samples was also investigated. Samples like those used in the *ex vivo* mechanical testing were soaked in DI water for 10 min, followed by loading into the MT. For both the 'humidifier off' and 'humidifier on' conditions, the Young modulus of the NC as a function of time removed from water was determined using the MT in dynamic mode. When the humidifier was not used to prevent the sample from drying, the Young modulus quickly increased to ∼400 MPa by the time the MT started, and after 5 min removed from the DI water, the Young modulus was ∼1100 MPa. When the humidifier was used, the Young modulus remained <100 MPa for nearly 4 min, and levelled out at ∼600 MPa after 7 min. It should be noted that the linear portion of the stress–strain curve was complete within ∼30 s after the start of the *ex vivo* mechanical testing. At this point, the sample had been removed from the brain for no more than 3 min, a time at which there would be a considerable increase in Young's modulus from drying if the humidifier were not used.

3.5. Buckling and insertion of neat and NC polymers

A summary of the recorded forces during the computer-controlled movement of both types of microprobes was created (figure 5). Measurements were made in one animal by alternating between microprobe types. To ensure that the microprobes were responding to just the cortical tissue, the surface of the brain was not supplemented with moisture and slowly dried during these experiments. As a result, the critical insertion force increased during the experiment. However, the graph (figure 5) demonstrates that the unreinforced (neat polymer) microprobes failed to insert into the cortical tissue at a lower critical force than the mechanically reinforced dynamic microprobes.

Using the device dimensions and Young's modulus of the neat or NC polymer, a critical buckling force was predicted using Euler's buckling formula:

$$F_{\text{crit}} = \frac{\pi^2 E I}{L_{\text{eff}}^2} \tag{2a}$$

and:

$$I = \frac{wt^3}{12}, \tag{2b}$$

where F_{crit} is the critical force required to buckle the implant, I is the area moment of inertia, w is the width, t is the thickness, E is the Young modulus of the material and L_{eff} is the effective length. The implant was modelled as a beam with one fixed end, and one hinged end, thus making $L_{\text{eff}} = \text{length}/\sqrt{2}$. For these calculations, the thickness is defined as being less than or equal to the width.

The critical buckling force is plotted as a grey horizontal bar where the standard deviation of sample dimensions

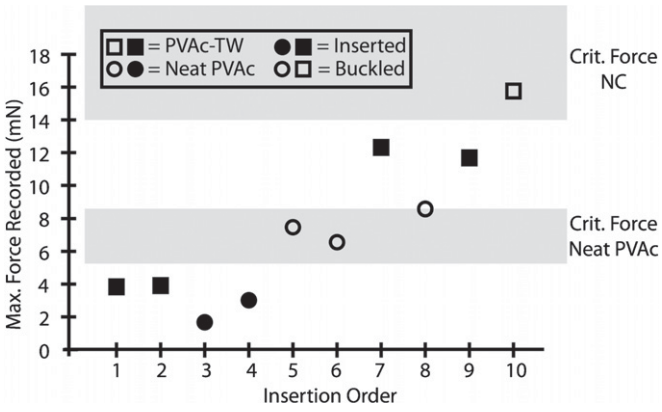

Figure 5. The maximum force was recorded by a computer-controlled load cell during each insertion attempt. The critical insertion force increased with subsequent trials. The circles represent neat PVAc microprobes, while the squares represent dynamic microprobes. Filled shapes were inserted successfully while open shapes buckled. The grey bars represent the critical buckling force (F_{crit}) for the microprobe, the theoretical maximum force the microprobe could endure before buckling. The F_{crit} is based on the material's modulus and measured dimensions with standard deviation. The height of the grey bars is determined by the standard deviation of the microprobe width and thickness.

determines the bar's height in figure 5. Although the NC microprobes are thinner than the neat polymer, the critical force of the NC is much higher because of the NC's greater Young's modulus. For both polymers, insertions were successful when the maximum force was less than the critical buckling force as predicted by Euler's buckling formula. When the maximum force exceeded the critical buckling force, microprobes would buckle. The NC was able to withstand a buckling force greater than the neat polymer (figure 6, supplementary movie 1, available at stacks.iop.org/JNE/8/046010/mmedia). Importantly, the neat polymer probes would need to be significantly bigger than NC microprobes, as a neat microprobe would need to be almost 40% thicker or three times wider than NC microprobes to allow insertion.

To better examine the functional consequences of the change in modulus of the dynamic NC, NC microprobes were implanted for several minutes. A NC microprobe was removed from the brain and attempted to be reinserted through intact pia. The computer-controlled reinsertion resulted in a typical buckling behaviour as the probe started to bow out, then buckle and collapse upon itself (figure 7, supplementary movie 2, available at stacks.iop.org/JNE/8/046010/mmedia).

3.6. Implanted NC microprobe histology

To examine the chronic inflammatory-mediated tissue response to the NC microprobes, we performed standard histological methods on animals that had been implanted with microelectrodes and allowed to survive for four or eight weeks. Classic haematoxylin and eosin (H+E) staining was performed on horizontal tissue sections from animals that had been implanted for eight weeks (figure 8(a)). Cell nuclei were stained by haematoxylin and are pictured as black dots and

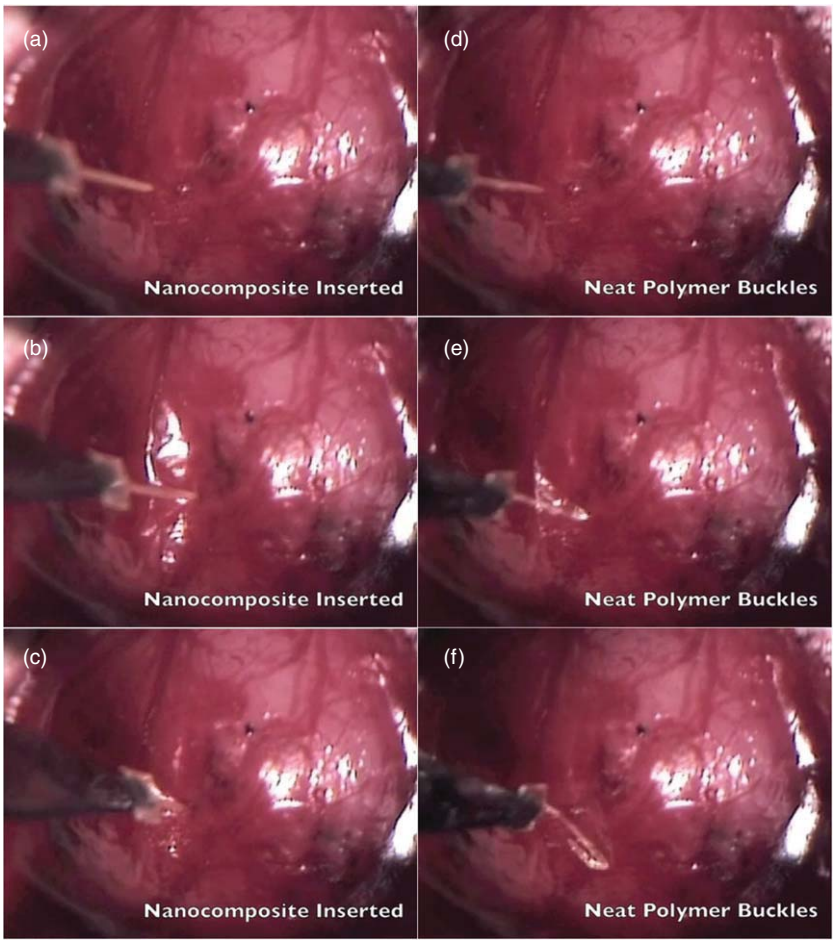

Figure 6. Snapshots of the supplementary movie 1 (available at stacks.iop.org/JNE/8/046010/mmedia) of insertion attempts of the neat polymer and the NC microprobes. (a) Before initial insertion, the NC is about a millimetre above the brain's surface. (b) During the movement, the NC indents and then penetrates the pia and cortex. (c) After the completion of movement, the NC is implanted in the brain and the indentation is relaxed. (d) Before initial insertion, the neat polymer is about a millimetre above the brain's surface. (e) During the movement, the neat polymer indents the pia but quickly buckles. (f) After the completion of movement, the neat polymer is completely buckled.

light black dots. The surrounding cortical tissue stained by eosin is pictured as grey, and blood vessels are throughout the section and appear as white holes. The image with NC still embedded in the section shows intimate contact of the tissue with the microprobe. The NC appears striated as a result of the ethanol dehydration during tissue processing. The dark ring around the NC shows increased density of cells at the tissue–microprobe interface. The response suggests the lack of significant necrosis or gliosis around the implant. Histological staining for total cell nuclei with DAPI (figure 8(b)) supports our finding from H+E staining. In this case, the NC was removed before DAPI imaging.

4. Discussion

In this study, we have for the first time been able to validate the feasibility of our mechanically adaptive NC as a microprobe that could form the basis of an intracortical microelectrode. We have shown the applicability of standard mechanics formulas in the insertion of microprobes. Euler's formula suggests that with our unique NC, we can decrease the size of the implant to minimize surgical trauma. Although this enables us to implant the material and understand its mechanical performance, we also demonstrated in preliminary histology studies that the implant does not create a significant glial scar. Collectively, this work lays the foundation for continued cortical electrode development to improve cortical neural recordings.

While our initial interest was in exploiting our dynamic mechanical materials in biomedical applications, specifically as adaptive substrates for intracortical microelectrodes, exposure to brain tissue had previously only been simulated by immersing the samples into ACSF and heating to a physiological temperature of 37 °C (Capadona *et al* 2008, Shanmuganathan *et al* 2009, 2010a, 2010b). Therefore, to examine the performance in the rodent brain, we used a MT that was developed specifically to test the small microprobes that have been developed towards intracortical microelectrodes. Previous results have validated that the MT provides similar results to DMA testing, a standard in the mechanical testing field (Hess *et al* 2009, 2011). Since the microprobes quickly change in response to temperature and water uptake (Capadona *et al* 2008), we were concerned that

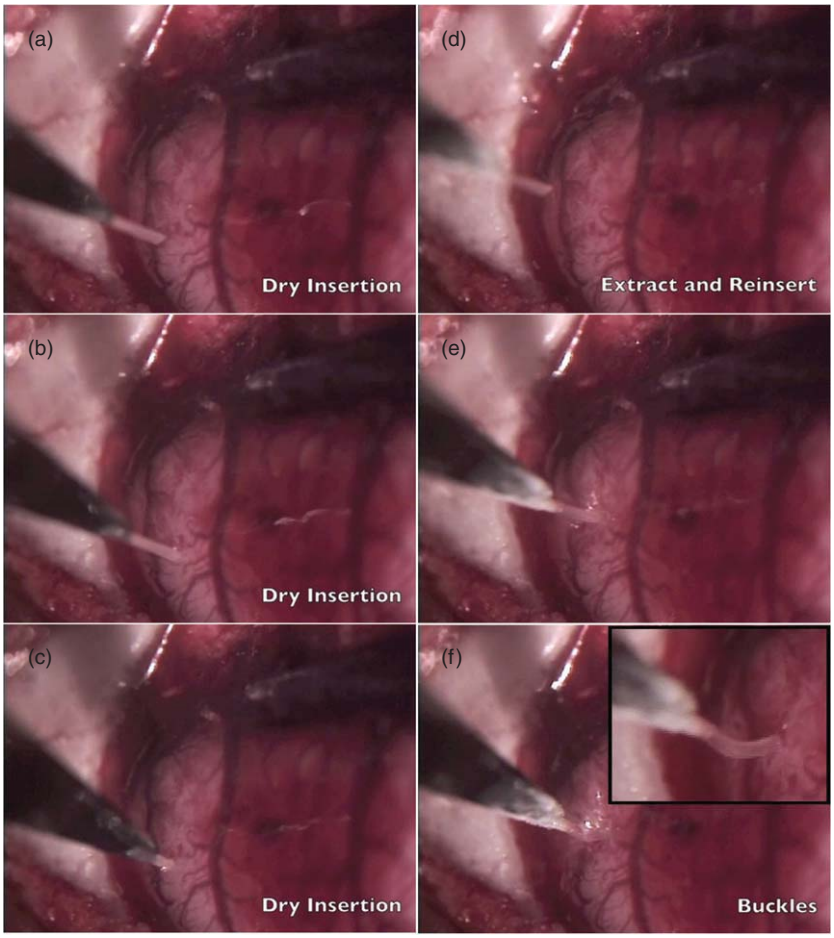

Figure 7. Snapshots of the supplementary movie 1 (available at stacks.iop.org/JNE/8/046010/mmedia) of insertion, retraction and buckling of the NC probe. (a) Before initial insertion, the NC is about a millimetre above the brain's surface. (b) During the movement, the NC indents and then penetrates the pia and cortex. (c) After the completion of movement, the NC rests in the brain for 3 min. (d) The NC is removed, and moved to a new location above the cortex. (e) During the movement of the reinsertion, the brain-softened NC indents the pia and cortex. (f) The NC is not stiff enough to puncture the pia and cortex, and the NC buckles. The inset depicts the close-up of curved buckled microprobe when removed from the brain's surface.

small samples would dry out once explanted from the rat brain. Therefore, the MT was paired with an airbrush and heat lamp to minimize drying and cooling when implants were removed from the brain (figure 1).

Our *ex vivo* MT confirmed that the NC rapidly decreases its modulus when implanted into the rodent brain (figure 4). Although the fabrication method provides some variability between samples, results consistently showed that the modulus switch occurred within the span of 5 min. Both DMA and MT testing showed similar modulus decreases, though DMA testing showed a more gradual change. The rate at which the dynamic material decreased its modulus was measured on the MT after extraction from the cortical tissue (figure 4), and compared to the bulk samples measured in the solution on a DMA. Differences are presumably due to the much larger surface-area-to-volume ratio of the micromachined samples used with the MT (Hess *et al* 2009, 2011, Capadona *et al* 2008). Additionally, for DMA measurements, dry samples were placed into a submersion clamp system to measure the dynamic change in modulus as the material both heated and swelled to decouple the reinforcing network and lower the modulus. In the DMA studies, the change in the dimensions of the material was not taken into account during swelling. This may account for slight difference in modulus between the two methods of testing.

Although we have confirmed that the material reduces its modulus once implanted, it is important to optimize the design of the electrode to minimize surgical trauma. Some research has suggested that microelectrode size does not affect the inflammatory tissue response (Szarowski *et al* 2003), yet other research has shown that very small electrodes do reduce the glial scar response (Seymour and Kipke 2007). Collectively, the recent literature suggests that size differences on the same order of magnitude are negligible while orders of magnitude size differences are significant factors in the glial scar response. Therefore, if the microelectrode size can be significantly minimized, through the use of proper design or new materials, one would be able to reduce the surgical trauma, presumably contributing to a decreased chronic inflammatory reaction.

Using design principles and methods, we sought to minimize the size of the implant needed for insertion by

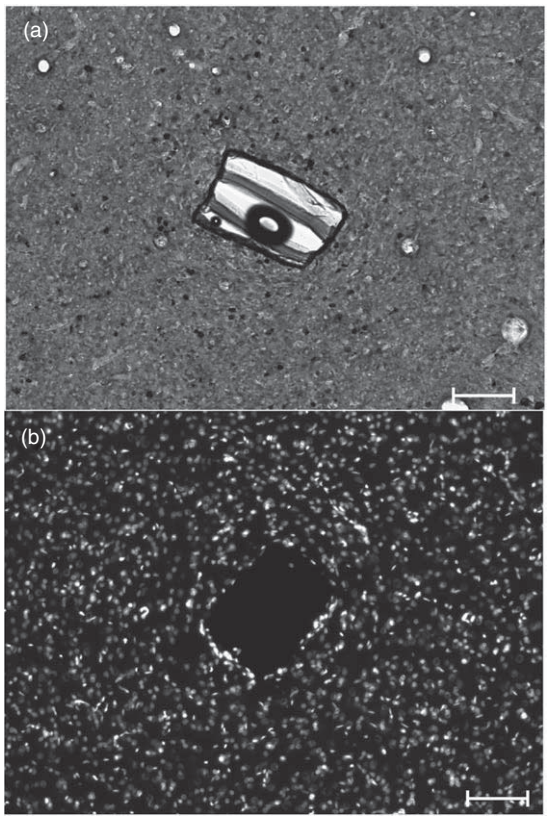

Figure 8. Histological evaluation of the microprobe–tissue interface was obtained with (a) H+E and (b) fluorescent staining with DAPI. All images were obtained from horizontal sections of brain tissue approximately 1 mm deep into the cortex of animals implanted for four (b, DAPI) or eight (a, H+E) weeks. (a) Nuclei are stained with various shades of black, other tissue is gray and blood vessels are white holes. (b) Fluorescent view of DAPI. Cell nuclei are pictured white (scale = 100 μm).

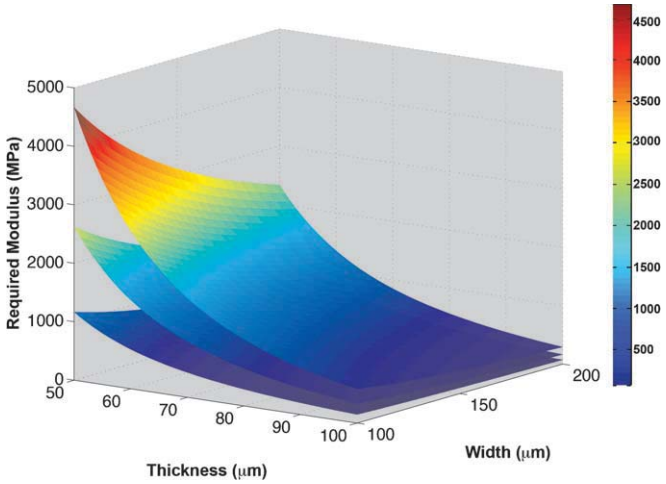

Figure 9. Parameter space for microprobe insertions. Based on a given force, the length, width and thickness are parameters for Euler's buckling formula to create a manifold to examine the required Young's modulus to prevent buckling and enable insertion into the rat cortex. The highest plane has a length of 4 mm, the next highest a length of 3 mm and the lowest plane a length of 2 mm. The scale bar represents modulus in MPa.

first measuring the required insertion force. We implanted microprobes into the cortex of many animals. Through the use of our custom computer-controlled inserter and force measurements, our experiments have shown that our hand-cut NC microprobe (100 μm thick, 200 μm wide) provides a range of insertion forces from 1.26 to 3.35 mN (95% confidence interval). Alternatively, the mean force for insertion is 2.30 mN $\pm$ 0.38 mN (standard error). The range of animal sizes varied from 206 to 335 g, but there was no correlation between animal size and required insertion force. A lack of correlation between size and force also occurred in prior pilot tests of the NC microprobe where the animal range was 227–353 g (data not shown).

Given the expected maximum insertion force, we can use the classical mechanical formula, Euler's buckling formula (equation (2*a*)), to compute the required modulus to ensure a buckle-free implantation into the cortex. Figure 9 shows the calculated modulus based on different device sizes (length, width and thickness). It is apparent that thickness is the main factor in buckling (figure 9). Theoretical microprobes above a given plane would insert, while microprobes below would buckle. It is also notable that the material modulus needed increases rapidly at smaller dimensions; this important factor has dictated that current standard cortical microelectrodes be made out of stiff metal or silicon (Schwartz 2004).

At the dimensions investigated in this study, both implants easily inserted into the cortex at low insertion force less than ~5.6 mN (figure 5). This is consistent with the findings of Najafi *et al.* Their study reported a penetration stress through the rat pia of 1.2×10^7 dynes cm^{-2} for a Si probe that was 40 μm in thickness and 80 μm in width, corresponding to a penetration force of 3.84 mN (Najafi and Hetke 1990). Figure 5 also clearly denotes an increased insertion force for subsequent microprobe implantations. Unreinforced polymer microprobes were unable to penetrate the pia tissue when the insertion force reached ~7 mN, while the mechanically reinforced dynamic NC microprobes were capable of penetrating the pia tissue with above 12 mN of force applied; both are consistent with predictions from Euler's buckling formula. The difference compared to the Najafi study was likely a result of our experimental conditions. Specifically, due to the rate at which the novel materials uptake moisture and decouple the reinforcing network resulting in significant decreases in modulus (see above and Capadona *et al* (2008), Shanmuganathan *et al* (2009), (2010a), (2010b)), it was important to ensure that the microprobes were responding to the cortical tissue, and not the increased moisture on the surface of the brain. Thus, the brain was not supplemented with moisture between trials. Unfortunately, over the time course of repeated implantations, the surface of the brain slowly dried and collected dried blood, and most likely increased in the elastic modulus of the pia. As a result, the critical insertion force increased during the experiment. While the absolute values for the force recorded during the critical insertion are not reflective of a single insertion model, figure 5 clearly demonstrates that the unreinforced (neat polymer) microprobes failed to insert into the cortical tissue before the mechanically reinforced dynamic microprobes.

The polymer NC consists of a controllable structural scaffold of rigid nanofibres embedded within a soft polymeric matrix. The network becomes the load-bearing element and leads to a high overall stiffness of the NC, as compared to the neat polymer materials. Therefore, the microprobes created from the dynamic materials are capable of sustaining an increased force during insertion. The improved mechanical properties of the NC over the neat polymer would therefore allow for a smaller device. As discussed above, to enable the insertion of a neat microprobe, the device would need to be almost 40% thicker or three times wider than NC microprobes to allow insertion.

In conjunction with the Boolean-type inserted/buckled results, we captured video of movements to show the complete functional impact of the properties of our NC. As shown above, the NC withstands greater insertion forces; demonstrated by videos showing the neat polymer buckle, directly followed by the insertion of the NC in the same area of brain (figure 6 and supplementary movie 1, available at stacks.iop.org/JNE/8/046010/mmedia). Additionally, the decrease in the modulus of the dynamic microprobe can be readily viewed by the naked eye within only a few minutes of the NC being implanted into the rat cortex. When the NC is then extracted and moved to another spot on the brain, due to the rapid decrease in modulus, the microprobe buckles and fails to penetrate into the pia tissue and reinsert into the cortical tissue (figure 7, supplementary movie 2, available at stacks.iop.org/JNE/8/046010/mmedia). The time between the two insertions attempts was of the order of tens of seconds. The drying of pia was minimal since the dry NC implanted with a force of 2.8 mN followed by the NC (after remaining in the brain for a few minutes) buckled upon reinsertion at about 3mN. These numbers agree well with what is predicted from the formulas.

Although we have shown how the properties of the brain influence the microprobe and its design, it is also important to examine the response of the brain tissue to the microprobe. In preliminary studies, we have used standard histological stains to investigate the material–tissue interface, with special interest in examining potential tissue necrosis. Histological staining of rats that had been implanted with dynamic NC microprobes and allowed to survive for four or eight weeks post-implantation suggests no tissue necrosis as a result of the implanted materials (figure 8). Further, both H+E and DAPI staining clearly show cell bodies at the implant interface, without excessive overgrowth, suggesting the lack of excessive glial scar tissue formation. Obviously, the extent of the histological examination presented on this tissue is not robust enough to fully understand the cortical tissue response to our novel bio-inspired mechanically dynamic microprobes. It is also important to point out that while this current generation of our dynamic NCs is capable of reducing its storage modulus to 12 MPa, the cortical brain tissue has been reported on the kPa range. However, *in silico* research has shown that a soft substrate on the order of 6 MPa significantly decreases the strain on surrounding tissue by up to two orders of magnitude in comparison to silicon ($E = 200$ GPa) or polyimide electrodes ($E \sim 3$GPa) (Subbaroyan *et al* 2005). Therefore, further studies are underway to examine the more detailed response to these materials, including a complete time course to examine the various stages of inflammation, as well as specific cellular (neuronal cell nuclei, astrocytes and microglia) and extracellular markers.

5. Conclusions

The goal in this work was to investigate the first biomedical application of our novel bio-inspired mechanically dynamic polymer NCs. The intrinsic properties of our materials were designed with the intended application of penetrating intracortical microprobes and to afford us the distinctive opportunity to investigate the role of material stiffness in the tissue response to the implant. Our previous work has clearly characterized the materials properties of our novel class of material, in a controlled laboratory setting. Here, we have for the first time validated these bench-top studies, and have shown the initial feasibility of our material towards an intracortical microelectrode. Specifically, we have shown that the dynamic polymer NC is sufficiently stiff to penetrate the cortical tissue without the need for assistive devices. Further, the initially stiff microprobe utilizes the *in vivo* environment to rapidly become compliant to more closely match the surrounding cortical tissue while initial histological examination suggests cellular integration at the microprobe–tissue interface. Taken collectively, this work has established a solid foundation to complete further studies to investigate the effect of substrate stiffness on glial scar formation and brain tissue response.

Acknowledgments

This work was supported by grant numbers R21-NS053798 and F31-NS063640 from the National Institute of Neurological Disorders and Stroke and T32-EB004314-06 for the National Institute of Biomedical Imaging and Bioengineering. Additional support was from the Department of Veterans Affairs grant numbers C3819C, F4827H and B6344W, as well as the National Science Foundation under grant number ECS-0621984. The authors acknowledge the support of Anne DeChant and Kadhirivan Shanmuganathan. None of the funding sources aided in the collection, analysis and interpretation of data, in the writing of the report, or in the decision to submit the paper for publication. The authors have no conflicts of interest related to this work to disclose.

References

Biran R, Martin D C and Tresco P A 2005 Neuronal cell loss accompanies the brain tissue response to chronically implanted silicon microelectrode arrays *Exp. Neurol.* **195** 115–26

Buzsáki G 2004 Large-scale recording of neuronal ensembles *Nat. Neurosci.* **7** 446–51

Capadona J R, Shanmuganathan K, Trittschuh S, Seidel S, Rowan S J and Weder C 2009 Polymer nanocomposites with nanowhiskers isolated from microcrystalline cellulose *Biomacromolecules* **10** 712–6

Capadona J R, Shanmuganathan K, Tyler D J, Rowan S J and Weder C 2008 Stimuli-responsive polymer nanocomposites inspired by the sea cucumber dermis *Science* **319** 1370

Capadona J R, Van Den Berg O, Capadona L A, Schroeter M, Rowan S J, Tyler D J and Weder C 2007 A versatile approach for the processing of polymer nanocomposites with self-assembled nanofibre templates *Nat. Nanotech.* **2** 765–9

Fernandez L J, Altuna A, Tijero M, Gabriel G, Villa R, Rodriguez M J, Batlle M, Vilares R, Berganzo J and Blanco F J 2009 Study of functional viability of SU-8-based microneedles for neural applications *J. Micromech. Microeng.* **19** 025007

He W and Bellamkonda R V 2008 *Indwelling Neural Implants: Strategies for Contending with the In Vivo Environment* ed W M Reichert (Boca Raton, FL: CRC)

Hess A, Capadona J, Shanmuganathan K, Hsu L, Rowan S, Weder C, Tyler D and Zorman C 2011 Development of a stimuli-responsive polymer nanocomposite toward biologically-optimized, MEMS-based neural probes *J. Micromech. Microeng.* **21** 054009

Hess A, Dunning J, Harris J, Capadona J R, Shanmuganathan K, Rowan S J, Weder C, Tyler D J and Zorman C A 2009 A bio-inspired, chemo-responsive polymer nanocomposite for mechanically dynamic microsystems *Solid-State Sensors, Actuators and Microsystems Conf., 2009. TRANSDUCERS 2009. International* pp 224–7

Hochberg L R, Serruya M D, Friehs G M, Mukand J A, Saleh M, Caplan A H, Branner A, Chen D, Penn R D and Donoghue J P 2006 Neuronal ensemble control of prosthetic devices by a human with tetraplegia *Nature* **442** 164–71

Jensen W, Yoshida K and Hofmann U G 2006 *In vivo* implant mechanics of flexible, silicon-based ACREO microelectrode arrays in rat cerebral cortex *IEEE Trans. Biomed. Eng.* **53** 934–40

Kee-Keun L *et al* 2004 Polyimide-based intracortical neural implant with improved structural stiffness *J. Micromech. Microeng.* **14** 32

Kennedy P R, Kirby M T, Moore M M, King B and Mallory A 2004 Computer control using human intracortical local field potentials *IEEE Trans. Neur. Syst. Rehabil. Eng.* **12** 339–44

Kozai T D and Kipke D R 2009 Insertion shuttle with carboxyl terminated self-assembled monolayer coatings for implanting flexible polymer neural probes in the brain *J. Neurosci. Methods* **184** 199–205

Leach J, Achyuta A K H and Murthy S K 2010 Bridging the divide between neuroprosthetic design, tissue engineering and neurobiology *Front. Neuroeng.* **2** 1–9

Lee H, Bellamkonda R V, Sun W and Levenston M E 2005 Biomechanical analysis of silicon microelectrode-induced strain in the brain *J. Neural Eng.* **2** 81

Lee K, He J, Clement R, Massia S and Kim B 2004 Biocompatible benzocyclobutene (BCB)-based neural implants with micro-fluidic channel *Biosens. Bioelectron.* **20** 404–7

Lee K-K, He J, Singh A and Kim B 2003 Benzocyclobutene (BCB) based intracortical neural implant *Proc. 2003 Int. Conf. on MEMS, NANO and Smart Systems* pp 418–22

Lillie R D 1965 *Histopathologic Technic and Practical Histochemistry* (New York: McGraw-Hill)

Lu Y, Wang D, Li T, Zhao X, Cao Y, Yang H and Duan Y Y 2009 Poly(vinyl alcohol)/poly(acrylic acid) hydrogel coatings for improving electrode-neural tissue interface *Biomaterials* **30** 4143–51

McConnell G C, Rees H D, Levey A I, Gutekunst C A, Gross R E and Bellamkonda R V 2009 Implanted neural electrodes cause chronic, local inflammation that is correlated with local neurodegeneration *J. Neural Eng.* **6** 056003

McConnell G C, Schneider T M, Owens D J and Bellamkonda R V 2007 Extraction force and cortical tissue reaction of silicon microelectrode arrays implanted in the rat brain *IEEE Trans. Biomed. Eng.* **54** 1097–107

Mercanzini A, Colin P, Bensadoun J C, Bertsch A and Renaud P 2009 *In vivo* electrical impedance spectroscopy of tissue reaction to microelectrode arrays *IEEE Trans. Biomed. Eng.* **56** 1909–18

Najafi K and Hetke J F 1990 Strength characterization of silicon microprobes in neurophysiological tissues *IEEE Trans. Biomed. Eng.* **37** 474–81

Nicolelis M A 2003 Brain–machine interfaces to restore motor function and probe neural circuits *Nat. Rev.* **4** 417–22

Nikles S A, Pellinen D S, Kitagawa J, Bradley R M, Kipke D R and Najafi K 2003 Long term *in vitro* monitoring of polyimide microprobe electrical properties *Engineering in Medicine and Biology Society, 2003. Proc. 25th Annual Int. Conf. of the IEEE***vol 4** pp 3340–3

Paralikar K J, Lawrence J K and Clement R S 2006 Collagenase-aided insertion of intracortical microelectrode arrays: evaluation of insertion force and chronic recording performance *Engineering in Medicine and Biology Society, 2006: EMBS '06. 28th Annual Int. Conf. of the IEEE* pp 2958–61

Polikov V S, Block M L, Fellous J M, Hong J S and Reichert W M 2006 *In vitro* model of glial scarring around neuroelectrodes chronically implanted in the CNS *Biomaterials* **27** 5368–76

Polikov V S, Tresco P A and Reichert W M 2005 Response of brain tissue to chronically implanted neural electrodes *J. Neurosci. Methods* **148** 1–18

R Development Core Team 2009 *R: A Language and Environment for Statistical Computing* (Vienna: R Foundation for Statistical Computing)

Rousche P J, Pellinen D S, Pivin D P, Williams J C, Vetter R J and Kipke D R 2001 Flexible polyimide-based intracortical electrode arrays with bioactive capability *IEEE Trans. Biomed. Eng.* **48** 361–71

Schwartz A B 2004 Cortical neural prosthetics *Annu. Rev. Neurosci.* **27** 487–507

Seymour J P and Kipke D R 2007 Neural probe design for reduced tissue encapsulation in CNS *Biomaterials* **28** 3594–607

Shanmuganathan K 2010 Bio-inspired stimuli responsive mechanically dynamic nanocomposites *Macromolecular Science and Engineering* (Cleveland, OH: Case Western Reserve University)

Shanmuganathan K, Capadona J R, Rowan S J and Weder C 2009 Stimuli-responsive mechanically adaptive polymer nanocomposites *ACS Appl. Mater. Interfaces* **2** 165–74

Shanmuganathan K, Capadona J R, Rowan S J and Weder C 2010a Bio-inspired mechanically-adaptive nanocomposites derived from cotton cellulose whiskers *J. Mater. Chem.* **20** 180

Shanmuganathan K, Capadona J R, Rowan S J and Weder C 2010b Biomimetic mechanically adaptive nanocomposites *Prog. Polym. Sci.* **35** 212–22

Subbaroyan J and Kipke D R 2006 The role of flexible polymer interconnects in chronic tissue response induced by intracortical microelectrodes—a modeling and an *in vivo* study *Conf. Proc. IEEE Eng. Med. Biol. Soc.* **1** 3588–91

Subbaroyan J, Martin D C and Kipke D R 2005 A finite-element model of the mechanical effects of implantable microelectrodes in the cerebral cortex *J. Neural Eng.* **2** 103

Szarowski D H, Andersen M D, Retterer S, Spence A J, Isaacson M, Craighead H G, Turner J N and Shain W 2003 Brain responses to micro-machined silicon devices *Brain Res.* **983** 23–35

Takeuchi S, Suzuki T, Mabuchi K and Fujita H 2004 3D flexible multichannel neural probe array *J. Micromech. Microeng.* **14** 104–7

Takeuchi S, Ziegler D, Yoshida Y, Mabuchi K and Suzuki T 2005 Parylene flexible neural probes integrated with microfluidic channels *Lab Chip* **5** 519–23

van den Berg O, Capadona J R and Weder C 2007 Preparation of homogeneous dispersions of tunicate cellulose whiskers in organic solvents *Biomacromolecules* **8** 1353–7

Ward M P, Rajdev P, Ellison C and Irazoqui P P 2009 Toward a comparison of microelectrodes for acute and chronic recordings *Brain Res.* **1282** 183–200
Wester B A, Lee R H and LaPlaca M C 2009 Development and characterization of *in vivo* flexible electrodes compatible with large tissue displacements *J. Neural Eng.* **6** 024002
Williams J C, Hippensteel J A, Dilgen J, Shain W and Kipke D R 2007 Complex impedance spectroscopy for monitoring tissue responses to inserted neural implants *J. Neural Eng.* **4** 410
Williams J C, Rennaker R L and Kipke D R 1999 Long-term neural recording characteristics of wire microelectrode arrays implanted in cerebral cortex *Brain Res. Protoc.* **4** 303–13